JOURNAL OF MATERIALS SCIENCE 11 (1976) 1794–1806

The mechanism of simultaneous sintering and phase transformation in alumina

P. A. BADKAR*, J. E. BAILEY
Department of Metallurgy and Materials Technology, University of Surrey, Guildford, Surrey, UK

The sintering behaviour of boehmitic alumina gels during the transformation to the stable α phase has been studied using dilatometry, transmission electron microscopy, X-ray analysis and differential thermal analysis. The specimens for transmission electron microscopy were prepared from gel specimens, sintered to various predetermined temperatures, using an ion-beam thinning technique. The transmission electron microscope study and X-ray analysis have revealed a characteristic sintering behaviour which is associated with the θ to α phase transition. The transformation to the α phase occurs by a nucleation and growth process. During the growth process considerable redistribution of the fine porosity existing within the transition alumina matrix occurs, in the form of large elongated interconnected pores trapped within the nucleating α grains. These pores grow rapidly to a size approximately one hundred times that of the θ grains. This process results in a rapid fall-off in sintering rate at the end of the transformation. A study of the θ/α interphase interface by transmission electron microscopy has led to the development of a model that accounts satisfactorily for the redistribution of the porosity.

1. Introduction

It is well known that aluminas derived from the decomposition of gelatinous boehmite and related hydroxide aluminas undergo a number of phase transformations before the stable α phase is obtained and the structures of so-called transition aluminas have been the subject of several investigations [1–3]. In general, alumina bodies are produced by the compaction and sintering of α alumina powders; there is, however, interest in alumina bodies produced directly by the compaction, subsequent decomposition and sintering of the boehmite and other hydrated aluminas. The reason for this is that alumina gels have a characteristic sintering behaviour [4–6] showing a region of enhanced sintering in the temperature range 1000 to 1200° C followed by a transition to a much reduced rate of densification in the temperature range 1200 to 1500° C. This behaviour is related to the phase transformations occurring in this temperature range and it has been shown that the transformation from θ to α alumina reduces drastically the rate of sintering which in the fine-grained θ alumina is extremely rapid.

The main purpose of the studies reported here was to determine the mechanism of sintering during the θ to α phase transition and thereby account, firstly, for the much reduced sintering rate on transformation to the α phase and, secondly, for the formation of the characteristic pore structure in the α alumina.

Transmission electron microscopy and related techniques have been used in the work in conjunction with differential thermal analysis and dilatometry measurements. This paper describes the detailed structural changes occurring during the simultaneous sintering and phase transformation, and a simple model is developed from these observations to account for the sintering behaviour and pore structure of the derived α aluminas.

---

*Present address: Denbyware Ltd, Derby, UK

2. Materials and experimental procedures

2.1. Materials

Balgel, doped with ∿ 0.25% MgO (by weight) was selected as the main alumina gel to be used. This material was supplied by AERA, Harwell. Apart from the intentionally added MgO, this material contained the following impurities (in ppm):

<20 CaO, <10 K_2O, <550 SO_3, <5 P_2O_5,

<90 SiO_2, <15 TiO_2, <5 V_2O_5, <5 MnO_2,

<40 Fe_2O_3, <100 MgO, <100 Ba_2O_3.

Initial examination of this material by scanning electron microscopy established that Balgel consists of spherical agglomerates 10 to 20 μm in size. These agglomerates could be readily dispersed in water, and electron microscopy showed that the dispersant consisted of particles 50 to 100 Å in size. X-ray line broadening suggested a crystallite size of about 60 Å.

A fibrillar boehmite (designated as Baymal) was used for comparison purposes. This material contained the following impurities:

9.8% acetic acid, 1.7% SO_3, 0.02% SiO_2,

0.015% Fe_2O_3 and 0.07% Na_2O.

It was confirmed that this material has a fibrillar structure [7] consisting of fibres 50 to 80 Å in diameter and 1000 to 2000 Å long.

2.2. Experimental

Powder compacts, 9.7 mm diameter x 2 mm thick, were prepared in a steel die at a pressure of 49.2 kg mm^{-2}. The density of all green and sintered compacts was determined by a mercury displacement method similar to that described by Ashworth [8].

Sintering experiments were carried out in a Leitz Wetzlar, model UBD, high-temperature dilatometer. The specimen was heated at a constant rate of 15° C min^{-1}. Dimensional changes in the compacts were recorded versus temperature on a photographic film. The dilatometer curves have been replotted in this paper as percentage linear shrinkage versus temperature.

X-ray analysis was carried out on compacts headed to predetermined sintering temperatures with a Debye–Scherrer PW 1024 (11.48 cm) powder camera, using a Ni-filtered Cu$K\alpha$ radiation. The sintered specimens were crushed and ground in an alumina mortar and pestle and the resulting powder was sieved through −200 mesh prior to analysis.

Quantitative DTA was carried out using a 'Standata 6.25' apparatus, ZrO_2 and α-alumina (1 μm particle size) were used as calibration and reference samples respectively. The test samples were diluted in the ratio 2:1 with the reference material. Two heating rates, 15 and 7.5° C min^{-1}, were used. The heat of enthalpy of the polymorphic phase change was calculated using the method of Cunningham and Wilburn [9].

The specimens cut from partially sintered materials were prepared for transmission electron microscopy by mechanical polishing in a suitable jig, followed by thinning in an "Edward high vacuum IBMA-I" ion-beam thinning machine, similar to that described by Barber [10]. The thinned specimens were examined in a JEOL 100B electron microscope equipped with a goniometer stage to facilitate tilting of the specimen within ± 30° about two orthogonal axes. It was found necessary to coat the thinned specimens with a thin layer of carbon to prevent them charging in the microscope. The charging was probably due to the very low electrical conductivity of alumina and high porosity content of the specimens.

3. Results

3.1. Dilatometry

The shrinkage curves for Balgel and Baymal are shown in Fig. 1. Both these curves are similar in outline. There are, however, certain differences in detail. Baymal showed a slight expansion in the temperature range 20 to 100° C, and the transition to a low shrinkage rate occurred at a higher temperature of ~ 1300° C, compared with ~ 1200° C for Balgel. Furthermore, it should be noted that the apparent high shrinkage of the Baymal compact is misleading since it showed anisotropic shrinkage (32% linear in thickness and 17% linear in diameter) whereas the Balgel compact shrunk nearly isotropically.

The room-temperature bulk densities of the Balgel and Baymal compacts sintered at the constant heating rate of 15° C min^{-1} to various predetermined temperatures are compared along with their green densities in Table I.

It is apparent from Table I that Baymal compacts show consistently lower densification than those of Balgel compacts during non-isothermal sintering. This was mainly due to the higher loss in mass of the Baymal compacts during dehydroxy-

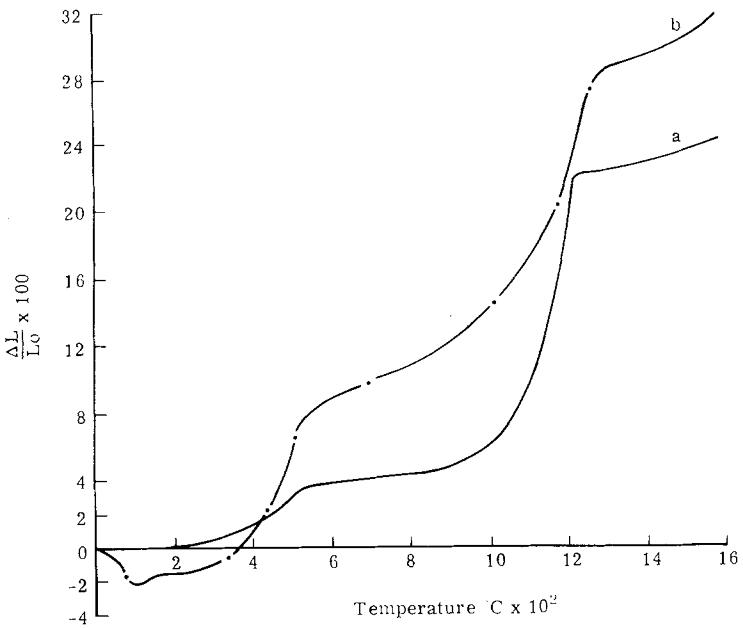

Figure 1 Dilatomeric shrinkage curves for (a) Balgel and (b) Baymal compacts. Heating rate 15° C min^{-1}.

TABLE I Room temperature bulk densities expressed as percentage of the theoretical density of the α-Al_2O_3

Temp.	Green	600° C	800° C	1000° C	1100° C	1150° C
Balgel	45.3	40.3	–	44.1	–	56.2
Baymal	42.8	–	39.2	–	41.2	–
Temp.	**1180° C**	**1200° C**	**1230° C**	**1270° C**	**1320° C**	**1600° C**
Balgel	63.2	70.3	–	–	–	73.6
Baymal	–	–	51.7	55.2	56.2	60.8

lation as this powder contained ~9.8% acetic acid; the higher weight loss in Baymal compacts was confirmed by thermogravimetric analysis.

3.2. X-ray analysis

The ASTM X-ray index and Lippens' [11] data were used to analyse the X-ray diffraction patterns obtained from the gel specimens sintered to various predetermined temperatures. The results are summarized in Table II.

TABLE II Summary of the crystalline phases observed in the non-isothermally sintered gel specimens

Sintering temperature (° C)	Crystallographic phase present	
	Balgel	Baymal
600	γ	γ
800	γ	γ
1000	δ	γ
1100	δ	θ
1150	$\delta + \theta$	θ
1170	$\alpha + \delta + \theta$	θ
1200	α + trace θ	θ
1230	α	$\theta + \alpha$
1270	α	$\theta + \alpha$
1320	α	α + trace θ

The phase transition sequence for the progressive conversion of the sintered Balgel compacts is the same as that observed for the calcined powders reported earlier [6]. Similarly, in the case of Baymal compacts, the absence of δ phase is in agreement with the results for calcined powders [2].

3.3. Differential thermal analysis

The differential thermal analysis (DTA) curves for the Balgel and Baymal powders are shown in Fig. 2. The curves show similar characteristics in most respects. There is a small endothermic peak at a temperature of 107° C followed by an exothermic peak in the temperature range 180 to 330° C, which differed in size for the two gels. A large endothermic peak is observed in the temperature range 475 to 485° C, and an exothermic peak in the temperature range 1220 to 1270° C. The Baymal sample, however, showed an additional reproducible exothermic peak at 520° C.

The low temperature endothermic peak has been attributed to the removal of absorbed moisture [12]. The X-ray analysis showed that at

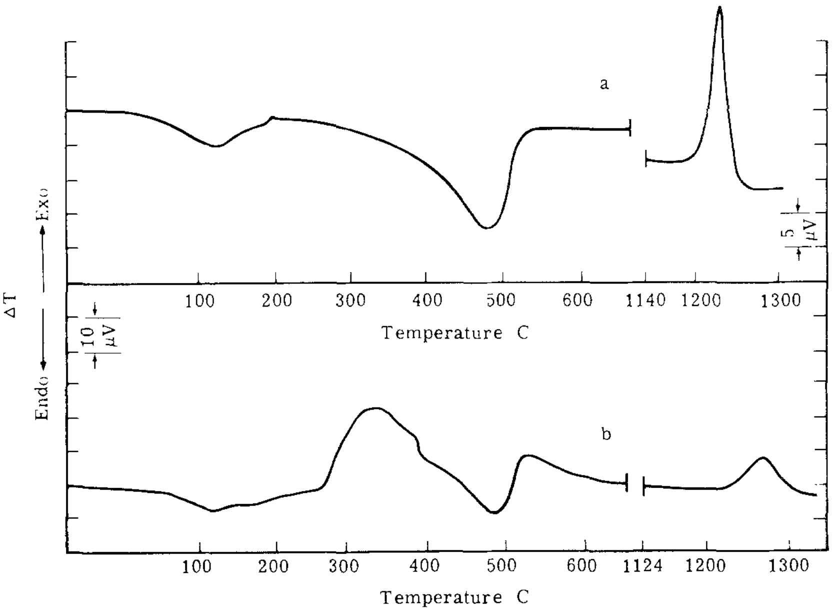

Figure 2 Differential thermal analysis curves for (a) Balgel and (b) Baymal powders. Heating rate 15° C min^{-1}.

600° C the gels are completely converted to γ alumina (Table II). Therefore, the second endothermic peak is clearly due to the loss of chemically combined water in the gels. The shape of the peak suggests that water of hydration is lost over a comparatively wide range of temperature.

The exothermic peak observed in the temperature range 1220 to 1270° C is due to the transition to α alumina as confirmed by the X-ray analysis (Table II). The exothermic peak for Balgel is large and sharp, and occurs at 1220° C; in contrast, the peak is small, broad and shifted to a higher peak temperature of 1270° C for the Baymal powder.

A major difference found between these gels concerned the exothermic peak in the temperature range 180 to 330° C. The Baymal powder shows a broad peak at 326° C, whereas the Balgel shows a very small peak at 188° C. The explanation for this peak is uncertain; however, it may be related to the anionic impurity content which is much greater for the Baymal Samples as can be seen from the chemical analysis. It is possible, therefore, that the peak is due to exothermic reactions of the anionic impurities. No explanation could be found, however, for the occurrence of an exothermic peak following the end of dehydroxylation in the Baymal powder.

The enthalpy values (ΔH_v) calculated from the final exothermic peak, and related to the θ to α phase transition, were estimated to be 3.4 ± 0.25 kcal mol^{-1} for Balgel and 1.8 ± 0.25 kcal mol^{-1} for Baymal. These values are comparable to those reported by Yakokawa and Kleppa [13], which are in the range 2.6 to 5.3 kcal mol^{-1}, for three different metastable aluminas. To test the experimental results with a geometrical model generated later (Section 3.3), it was necessary to obtain a value for the free energy of transformation ΔG_v. The correct value of ΔG_v can only be determined if the entropy of transition ΔS_v is known, since all these quantities are related by the following expression:

$$\Delta G_v = \Delta H_v - T\Delta S_v. \tag{1}$$

The θ to α phase transition is thermodynamically irreversible; therefore, the normal reversible thermodynamic approach to determine ΔS_v cannot be used. An indirect way to determine ΔG_v is to calculate the free energy of formation, ΔG_F, of both the phases at various temperatures and then to take the difference at any required temperature. Calculations of this kind have been carried out for the γ to α phase transition by Stull and Prophet, and reported in JANAF thermodynamic tables [14]. A detailed consideration of these tables [15] indicated that a reasonable assumption would be to take $\Delta G_v \simeq \frac{1}{2}\,\Delta H_v$ at the transformation temperature. On this basis, the derived values for ΔG_v for Baymal and Balgel are 0.9 and 1.7 kcal mol^{-1} respectively. The different values for ΔH_v and hence ΔG_v for the two gels are unexpected since both these powders finally transform to α via the θ phase.

There is no evidence from the thermal analysis for detectable enthalpy changes associated with the metastable alumina transitions (see also Plummer [16]). It is unlikely, therefore, that the transition from δ to θ to α in the case of Balgel could account for the difference. Surface energy differences were also considered but seemed unable to account for the difference in ΔH_v values of Baymal and Balgel. A satisfactory explanation could not be found for the difference in ΔH_v values of Baymal and Balgel and, for the purpose of the present paper, it seemed reasonable to take these values as upper and lower limits for ΔG_v.

It is important to point out that there must be a contribution to the heat evolved from the surface and grain-boundary energies released during the phase transformation. However, it is not possible to determine this contribution which is denoted as $\bar{\epsilon}_\theta$ in Equation 12, and therefore it is included in the value of ΔH_v above which means that the estimates of ΔG_v made above effectively include $\bar{\epsilon}_\theta$ and are regarded as estimates of $\Delta G_v + \bar{\epsilon}_\theta$ in this paper.

3.4. Electron microscopy

X-ray analysis indicated that Balgel specimens sintered at 15° C min^{-1} to 1180° C consisted of a mixture of δ, θ and α aluminas (Table II), and therefore a duplex structure is to be expected at this temperature; these specimens were examined by transmission electron microscopy. An electron micrograph is shown in Fig. 3a. The microstructure appears to consist of islands of "coarse" crystallites intermingled with pores (see A in Fig. 3a) surrounded by a porous matrix of very fine crystallites (see B in Fig. 3a). The areas indicated at A showed considerable variation in their size. However, it was not possible to obtain an

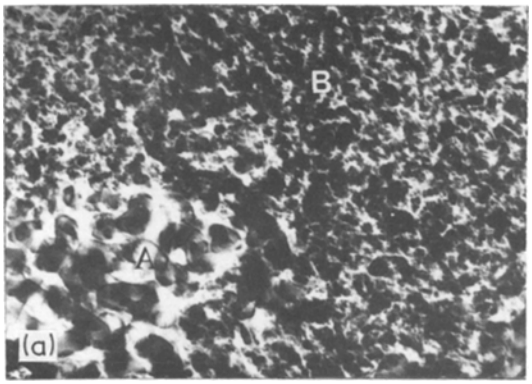

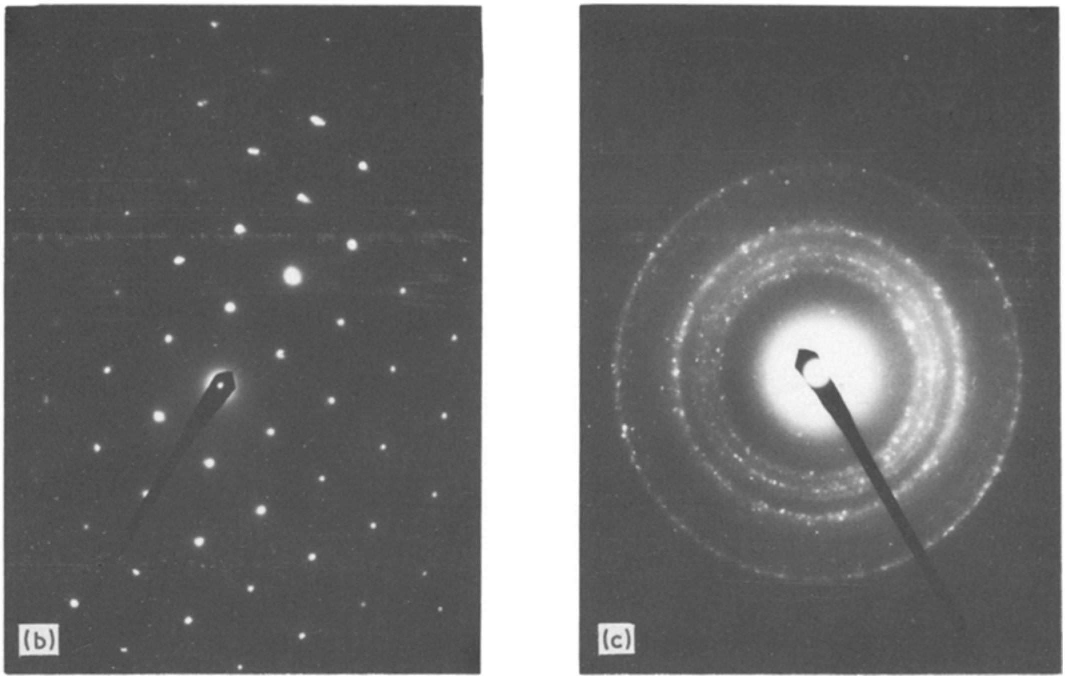

Figure 3(a) Electron micrograph of a Balgel compact sintered to 1180° C at a heating rate of 15° C min^{-1}, × 75 000. (b) Electron diffraction pattern taken from the area indicated at A. (c) Electron diffraction pattern taken from the area indicated at B.

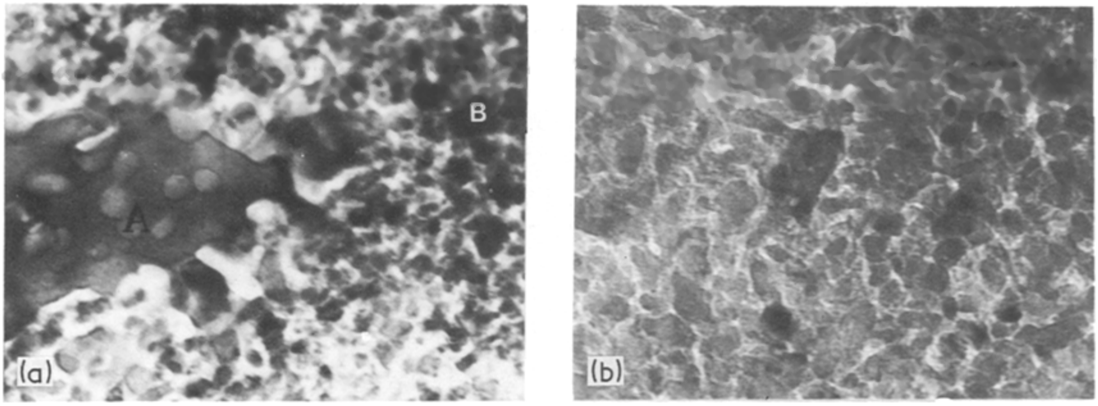

Figure 4(a) Electron micrograph of a Balgel compact, showing trapped porosity within the growing α grain, × 180 000. (b) Typical electron micrograph of the polycrystalline θ matrix, × 310 000.

average size since only small areas of the entire specimen could be thinned by the ion-beam thinning technique. Occasionally, areas which appeared distinctly as grains with pores trapped within them were also observed. A typical example is shown in Fig. 4a.

Electron diffraction patterns obtained from both regions A and B, using a selected-area diffraction aperture of 0.25 μm, are shown in Fig. 3b and c. The diffraction pattern of region A is a sharp single crystal pattern, which on analysis was shown to be α alumina, and there is only very little arcing or splitting of the diffraction spots. This observation is significant since it shows that regions similar to A in Fig. 3a, are not clusters of polycrystalline grains, as might well be concluded from a visual examination. Extensive scanning with a small selected-area diffraction aperture of regions similar to A (Fig. 3a) showed that, in general, the observed single crystal orientations changed discontinuously over distances in the range 1 to 2 μm; however, it was found extremely difficult to identify the grain boundaries between single crystal grains, and it was considered that this resulted from the varying contrast due to the porosity distribution within these grains. Furthermore the overlapping nature of the porosity made it difficult to estimate the pore size and spacing within the α grains. A visual estimation suggested a pore size in the range 600 to 1000 Å. It should be borne in mind, however, that at the high porosity levels observed, the pores are likely to be largely interconnected.

Electron diffraction patterns (Fig. 3c) from regions such as B in Fig. 3a became increasingly spotty on decreasing the diameter of the selected-area diffraction aperture, suggesting that these regions consist of fine discrete grains. The *d* spacings worked out from these rings corresponded well with those of the θ phase alumina. It should be noted, however, that in the case of Balgel specimens sintered to 1180° C, the X-ray analysis indicated a mixture of δ and θ phases. The apparent discrepancy in the X-ray and electron diffraction results is due to considerable overlapping of *d* spacings of the two phases and the insufficient resolution of the electron diffraction camera. The average grain size of the fine polycrystalline matrix was obtained at higher magnifications. A typical electron micrograph is shown in Fig. 4b. The general appearance of the structure is that of grains joined by necks and grain boundaries. A rough estimate of the average grain and pore size gave values of 260 ± 50 and 75 ± 25 Å, respectively. It should be pointed out, however, that these estimates are difficult to make owing to overlapping of fine grains and pores which are likely to give rise to contrast effects that can be interpreted as grain boundaries.

The microstructure of the Baymal specimens, in general, was similar to that of the Balgel specimens, as shown in Fig. 5a. The coarse structure regions, A, surrounded by the fine polycrystalline matrix, B, were observed. The electron diffraction pattern taken from within region A of Fig. 5a is shown in Fig. 5b and that taken from the fine matrix B alone is shown in Fig. 5c. As in the case for Balgel specimens, the electron diffraction patterns indicated that regions such as A are single crystal α alumina and regions such as B are poly-

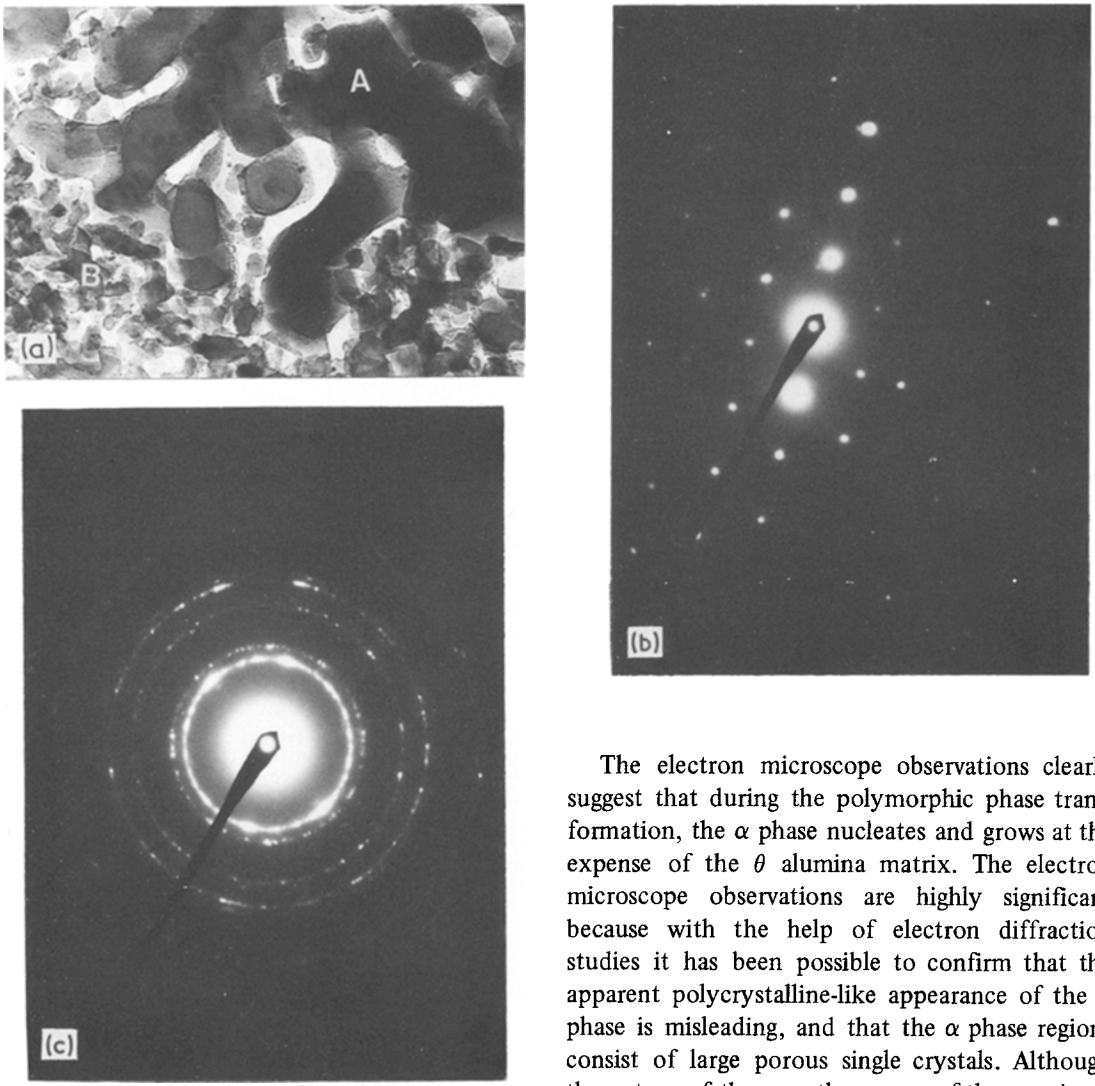

Figure 5(a) Electron micrograph of a Baymal specimen sintered to 1230° C at a heating rate of 15° C min^{-1}, × 125 000. (b) Electron diffraction pattern taken from the area indicated at A. (c) Electron diffraction pattern taken from the area indicated at B.

crystalline θ alumina. The pores within the α grains are similar in character and somewhat coarser in size compared with the single crystal regions of the Balgel specimens.

The polycrystalline θ matrix appears more porous than that observed for the Balgel specimen. This is in accordance with the difference between their relative bulk densities (Table II). Measurement of the average grain size of the θ grains in the Baymal specimen indicated an average value of 325 ± 50 Å. A rough estimation of the pore size indicated a value in the range 250 to 300 Å.

The electron microscope observations clearly suggest that during the polymorphic phase transformation, the α phase nucleates and grows at the expense of the θ alumina matrix. The electron microscope observations are highly significant because with the help of electron diffraction studies it has been possible to confirm that the apparent polycrystalline-like appearance of the α phase is misleading, and that the α phase regions consist of large porous single crystals. Although the nature of the growth process of the α grains is not clear from Fig. 3a, the micrograph does indicate that considerable redistribution of the fine pores present in the θ matrix occurs into larger pores. The nature of the growth process can be deduced from the micrographs shown in Figs. 4a and 5a. A close examination of Fig. 4a shows that some parts of the interface between the θ and α grains bulge out and grow preferentially on a fine scale producing what may be described as a finger-like growth. This finger-like growth is more clearly observed in Fig. 5a and the finger-like branches are seen to have widths in the range 600 to 1000 Å. The observed change in the porosity distribution would appear to result from the sweeping aside of the θ matrix porosity as the finger-like branches grow forward, thereby producing elongated pores, as depicted schematically in Fig. 6. It should be noted that during the phase transition, a volume

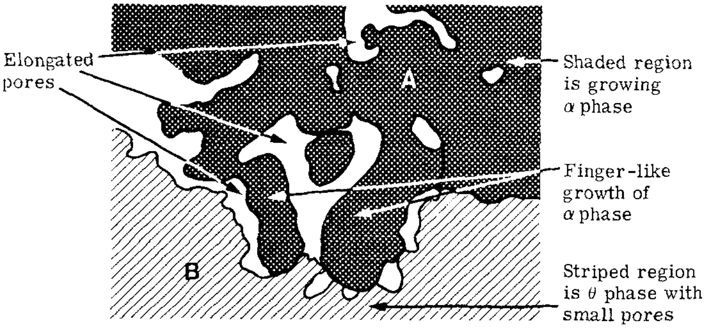

Figure 6 Schematic depiction of Fig. 5a.

contraction of approximately 8.5% occurs which has to be taken into account. It appears that this contraction is not accommodated merely by shrinking away of the α/θ interface from the matrix, since evidence of cracking at the interface was not observed. Strains created due to the volume contraction of the growing α grains may be relieved, therefore, by plastic flow in either the α or θ phase or both, or by diffusion processes at the interphase interface leading to pore closure and growth elsewhere.

In an attempt to study the development of α phase nuclei at an early stage of the transformation, Balgel specimens sintered at 1050° C for 6 h were thinned and examined on the electron microscope. Small isolated grains were observed (Fig. 7a), less than 1000 Å in diameter, and were identified from the electron diffraction to be α grains (Fig. 7b). Occasionally, even smaller grains were observed but these were not easily identifiable by the electron diffraction.

4. Discussion

4.1. α phase nucleation

The microstructural evidence presented in Section 3.4 clearly indicated that the phase transformation from θ to α phase occurred by a nucleation and growth mechanism. However, detailed evidence of the initial nucleation step could not be obtained. While small isolated α grains were observed ($\sim$ 1000 Å diameter, Fig. 7a) they were still large compared with the grain size and pore structure of the θ matrix. Attempts to relate grain nucleation to coarse irregularities in the structure were unsuccessful; for example, α grains were not observed specifically in the areas where the grain size of the θ grains was larger or smaller than average or non-uniform. Furthermore, amorphous regions were not observed, within which α grains would have nucleated, as has been reported by Iler [2]. The main difficulty in observing the initial nucleation stage in the sintered gel specimens is due to the problem of identifying a critical size α nucleus in the mass of polycrystalline θ matrix consisting of very fine crystallites ($\sim$ 200 to 300 Å). Electron diffraction patterns of very small α nuclei in the size range of polycrystalline θ matrix will not be strong enough to be recognized in the background of spotty diffraction rings obtained from the adjacent polycrystalline area. Thus a newly formed α grain will not be detectable until it grows to a sufficiently large size to give a

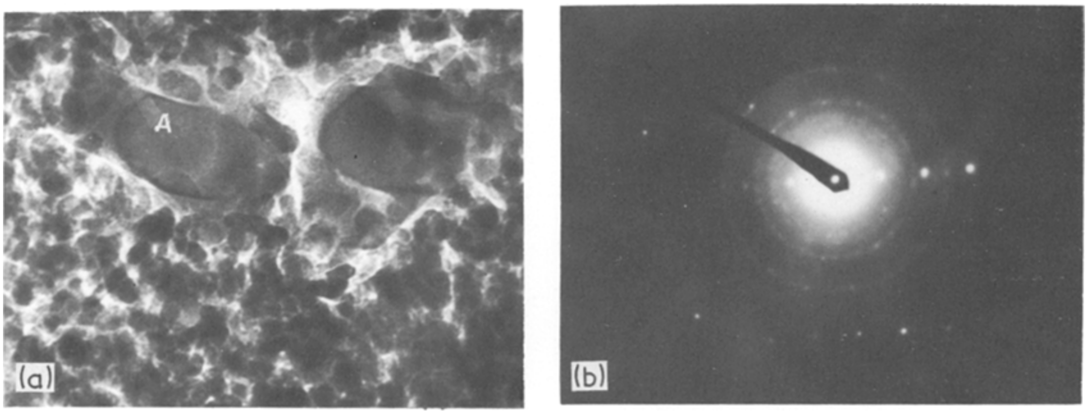

Figure 7(a) Electron micrograph of a Balgel specimen sintered at 1050° C for 6 h, showing α grains formed at an early stage of nucleation, X 200 000. (b) Electron diffraction pattern taken from the area indicated at A.

distinct single crystal diffraction pattern. However, the lack of any evidence to the contrary in these micrographs suggests that nucleation of the α phase occurs uniformly in the θ matrix, and on a scale that is coarse compared to the fine θ crystallite grain size, i.e. on average one α grain forms per 10^5 θ grains.

4.2. Growth of the α phase

Although the transmission electron microscope investigations gave very little information about the initial nucleation stage, it provided clear evidence (Figs. 3a, 4a and 5a) that during the growth of the α grains considerable redistribution of the fine interconnected porosity within the θ matrix occurs in the form of large elongated interconnected pores which are left within the growing α grains (e.g. Fig. 5a). It was pointed out in Section 3.4 that the α/θ interface migrates on a submicron scale in the form of finger-like branches and the submicron size of the fingers is relatively large ($\sim$ 500 to 1000 Å wide), compared to the crystallite size of the θ matrix ($\sim$ 250 to 350 Å diameter). These observations suggest that the fine pores within the θ matrix pin the α phase interface and for growth of the α phase to occur these pores must be removed.

A model can be envisaged for this process whereby the interface of the nucleating α grain is pinned by pores in the θ matrix. This is to be expected since the total interface energy can be reduced in much the same way as pores and inclusions pin grain boundaries [17]. Certain assumptions have to be made because it is clear from the electron micrographs of the θ matrix that the actual geometrical shapes of the θ grains are complex. For the purpose of development of a model it has been assumed that the pores between the θ grains and an α grain are toroidal in shape, and for simplicity it will be assumed that pores do not change their shape appreciably during the interface migration. This situation is depicted in Fig. 8, where it can be seen that any attempts of the interphase interface to migrate past the position AB will be opposed by the increase in the interfacial energy. The interface will migrate provided that the free energy of transformation released by the migration more than compensates for the increase in the interfacial energies.

The change in free energy, ΔF_V, will be given by:

$$\Delta F_\mathrm{V}\delta V = \gamma_{\alpha\theta}\delta A + (\gamma_\alpha - \gamma_\theta)\delta B - \Delta G_\mathrm{V}\delta V - \bar{\epsilon}_\theta \delta V, \qquad (2)$$

where $\gamma_{\alpha\theta}$ is the interphase interface energy, γ_α and γ_θ are the surface energies of the α and θ alumina phases, δA is the increase in the interphase interface area when the α alumina phase sweeps through a volume δV, and δB is the area of the pore surface swept over by the moving interface; ΔG_V is the free energy change per unit volume associated with the θ to α transformation, and $\bar{\epsilon}_\theta$ is the mean interfacial energy per unit volume within the θ matrix resulting from its polycrystalline and porous nature. Clearly migration will occur if

$$\Delta F_\mathrm{V}\delta V \leqslant 0,$$

i.e. using Equation 2 this condition becomes

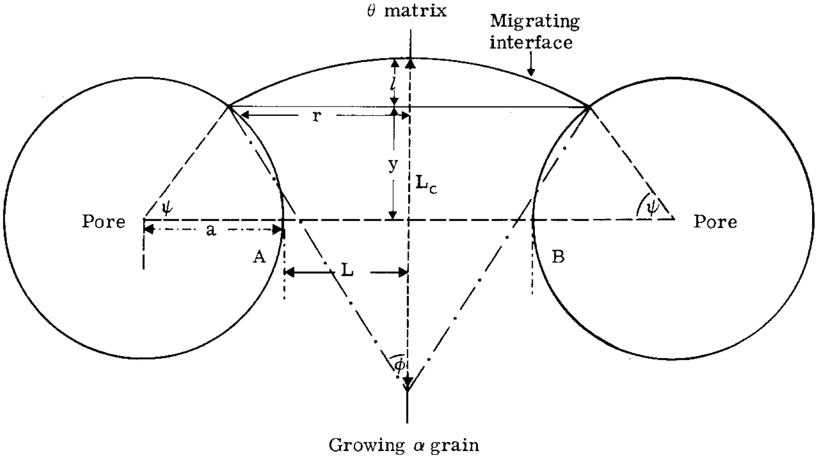

Figure 8 The model considered for the α phase growth, showing a cross-section through a toroidal pore.

$$(\Delta G_v - \bar{\epsilon}_\theta)\delta V \geqslant \gamma_{\alpha\theta}\,\delta A + (\gamma_\alpha - \gamma_\theta)\,\delta B. \quad (3)$$

It can be easily shown that if the interphase interface were pinned at its intersection with the toroidal pore AB (Fig. 8) then the driving force stemming from the free energy change $\Delta G_v + \bar{\epsilon}_\theta$ will cause the interface to bulge out until it reaches an equilibrium position at a radius L_c at which the energy release $(\Delta G_v + \bar{\epsilon}_\theta)\,\delta V$ just compensates for the increase in interfacial energy $\gamma_{\alpha\theta}\,\delta A$; we find

$$L_c = \frac{2\gamma_{\alpha\theta}}{\Delta G_v + \bar{\epsilon}_\theta} \quad (4)$$

Clearly the interface will not be hindered if $L > L_c$, where $2L$ is the distance AB. If $L < L_c$ then the spherical shape interface will bulge out to its equilibrium position at a radius of curvature L_c and it may then be possible for the interface to advance at constant radius of curvature past the toroidal pore as depicted in Fig. 8.

This model assumes that any constraint imposed on the shape of the interphase interface at the pore surface is small and does not appreciably distort the profile; this cannot be entirely true because, depending on the values of γ_α and γ_θ, the interphase interface will be in equilibrium at a fixed angle at the pore surface. Nevertheless, with this assumption and assuming further that $\gamma_\alpha \simeq \gamma_\theta$, we can simplify Equation 3 to determine what conditions would restrain the migration of the α grain interface for this model.

The condition for interface migration then becomes

$$(\Delta G_v + \bar{\epsilon}_\theta)\delta V - \gamma_{\alpha\theta}\delta A \geqslant 0, \quad (5)$$

and for the model this reduces to the condition (see Appendix Equation A6)

$$\frac{4\pi\gamma_{\alpha\theta}{}^2}{(\Delta G_v + \bar{\epsilon}_\theta)}\left(\cos^2\phi\tan\phi - \sin^2\phi\cot\psi\right) \leqslant 0$$

or $\tan\phi \geqslant \tan\psi$ $(\phi \neq 0)$

or $\phi \geqslant \psi$, (6)

for migration to occur, where the angles ϕ and ψ are defined in Fig. 8.

Since $L_c \sin\phi = L + a(1 - \cos\psi)$ and using inequality 6, then

$$L + a\,(1 - \cos\psi) \geqslant L_c \sin\psi;$$

this will be true for all ψ provided

$$L + a \geqslant L_c. \quad (7)$$

This model predicts, therefore, that the interphase interface cannot migrate past pores of the kind considered here unless $L + a \geqslant L_c$. The observation that the porosity is redistributed during the α phase growth suggests that the pore spacing $(L + a)$ in the θ matrix is less than L_c. A firm conclusion can only be drawn after a comparison has been made between the calculated value of $2L_c$ using Equation 4 and the average spacing between pore centres in the θ phase determined from the electron micrographs.

There are a number of difficulties in determining the average spacing between pore centres from the electron micrographs. The intercept method is difficult to apply because the nearest distance between pore centres is of interest. Therefore, the only possible way is to measure directly the spacing between pore centres, from selected pairs of pores, from the areas where pore neck geometrics are well resolved. However, this does not simplify the problem because of considerable overlapping of θ grains and overall poor resolvability of the fine θ matrix. Nevertheless, an attempt was made to measure these spacings from a number of electron micrographs which yielded a value of 150 ± 75 Å for the average spacing between pore centres.

To calculate $2L_c$ it is necessary to know the values of γ and ΔG_v with reasonable accuracy. Experimentally determined interfacial energy values for the α/θ interface are not known and could not be determined during the present investigation. However, most of the work carried out on interfacial energy measurements in two-phase metallic systems [17, 18] indicates interphase interface energy values are similar to high-angle grain-boundary energies in either of the phases. Since it is generally found that high-angle grain-boundary energies are approximately in the range 0.3 to 0.5 of surface energy values [19] it is reasonable to suppose that values for γ would also be in a similar range. The surface energy value for α alumina is reported to be approximately 1000 erg cm^{-2} [20], therefore it is expected that values for γ would be in the range 300 to 500 erg cm^{-2}. Since the value for $(\Delta G_v + \bar{\epsilon}_\theta)$ was expected to lie in the range 0.9 to 1.7 kcal mol^{-1}, i.e. 35.1 to 66.4 cal cm^{-3} (see Section 3.3) the calculation yields $2L_c$ in the range 40 to 130 Å. On comparing this calculated value with the experimentally determined one of 150 ± 75 Å, it is apparent that there is considerable overlap between the range of calculated and observed values. Bearing in mind the inaccuracies in the measurements, it is possible to conclude that the interface is pinned by the pores within the θ matrix.

However, it is necessary to consider whether it is possible to account for the porosity redistribution assuming that the interface is not obstructed by the pores and is free to migrate. The present electron microscope observations suggest that the pores adjacent to the interphase interface close relatively rapidly during the interface migration as compared to the closure of pores within the polycrystalline θ matrix. Thus if interphase interface migration occurs freely then it is necessary to show that redistribution of the porosity is possible in the time required for the interface to pass by the pores.

The interface will migrate at a linear rate in a direction x normal to itself at a rate given by [21]:

$$\frac{dx}{dt} = \frac{D_1}{kT}\frac{\Delta G_v}{\delta} \tag{8}$$

where D_1 is the effective diffusion coefficient for interface migration, k Boltzmann's constant, T temperature, ΔG_v the driving force, and δ width of the interface.

Therefore, the time t_i for the interface to migrate a distance of one pore diameter, $2r_0$, will be given by

$$2r_0 = \frac{D_1}{kT}\frac{\Delta G_v}{\delta}\,t_i. \tag{9}$$

To calculate the time required for closure of pores lying along the interface by vacancy migration, the following accepted expression derived by Kuczynski [22] may be used:

$$t_f = \frac{\pi kT r_0^4}{2\gamma v D_b \delta} \tag{10}$$

where t_f is the time for complete closure of pores of initial pore radius r_0, γ the specific surface energy, v the vacancy volume, and D_b the grain boundary diffusion coefficient.

Now from Equations 9 and 10 the ratio t_f/t_i is given by

$$\frac{t_f}{t_i} = \left(\frac{\pi}{4}\right)\left(\frac{D_1}{D_b}\right)\left(\frac{r_0^3}{\delta^2}\right)\left(\frac{\Delta G_v}{\gamma_v}\right) \tag{11}$$

Here it has been assumed that the interphase interface width δ is equal to one atomic spacing and is the same for atomic jumps normal and parallel to the interface. Clearly if pores are to close during interface migration then $t_f/t_i \leqslant 1$.

Taking $\Delta G_v = 1.7$ kcal mol^{-1} (1.2×10^{-13} erg/atom) (this value has been chosen from the experimentally determined values of ΔG_v, see Section 3.3); $\delta = 3 \times 10^{-8}$ cm, $v = 1.4 \times 10^{-23}$ cm^3; $\gamma = 1000$ erg cm^{-2} and $r_0 = 100 \times 10^{-8}$ cm, and putting $t_f \simeq t_i$, a value of 1.3×10^{-4} is deduced for the ratio D_1/D_b if pore closure is to occur. However, the literature suggests that diffusion coefficients perpendicular and parallel to an interface are of the same order of magnitude (see, for example, [21, 23, 24]. It is concluded, therefore, that it is unlikely that the observed porosity redistribution can be accounted for in this way, which gives additional support for the pinning model proposed.

4.3. Effect of the phase transformation on the sintering behaviour

The gel compacts undergo a rapid rate of densification in the temperature range 1000 to 1200° C for Balgel and 1000 to 1300° C for Baymal compacts, followed by a sharp drop in the densification rate of higher temperatures (see Fig. 1). The X-ray data (Table II) show that this sharp drop in sintering rate is associated with the transformation of the transition alumina to the stable α phase for both the Balgel and Baymal specimens. This important conclusion is further supported by the transmission electron microscopy and diffraction studies. As already described in Section 3.4, the nucleating single crystal α grains grow rapidly to a size approximately hundred times that of θ grains, and contain large amounts of trapped porosity. The transformation to the α phase therefore results in an α alumina structure of micron size grains containing approximately 25 to 35% by volume of interconnected porosity at temperatures in the range 1200 to 1300° C. The rapid fall-off in sintering rate on completion of the phase transformation can, therefore, be understood since a structure of this kind is not expected to sinter appreciably until much higher temperatures are reached. It is well established that pores trapped within α grains during the final stage of conventional sintering of α alumina are extremely difficult to remove [25, 26]. However, it is expected that the trapped porosity in the sintered gel specimens would be removed at higher temperatures as a result of the much finer grain size. Isothermal sintering experiments reported elsewhere [5] confirmed this behaviour and the associated reduction in porosity was observed at temperatures above 1500° C. This behaviour is also indicated in Fig. 1, where it can be seen that sintering rate is beginning to rise at temperatures above 1500° C. It is concluded, therefore, that the observed rapid densification of the gel compacts must be due to the fine polycrystalline θ matrix and the role of the θ to α phase transition is to inhibit rapid densification.

5. Conclusions

This study has shown that the characteristic rapid sintering exhibited by transition aluminas is inhibited by the transformation to the stable α phase. The transmission electron microscopy and associated diffraction studies have revealed that the transformation results in a microstructure that consists of micron size α grains containing a high degree of interconnected porosity (approximately 25 to 30% by volume). This resulting structure will only densify at higher sintering temperatures. The electron microscopy observations have also confirmed that the transformation from θ to α occurs by a nucleation and growth process and no transition amorphous phase has been detected during the phase transformation.

A model has been developed that accounts for the redistribution of the porosity during the interphase interface migration. The redistribution of the porosity results from effective pinning of the interphase interface by the θ phase porosity and it cannot migrate unless the pore spacing reaches a critical value, and even then for certain values of pore sizes compared to pore spacing, migration may not occur, as discussed in a previous section.

The microstructural studies demonstrate that while the initial rapid sintering rate of fine transition aluminas may seem attractive, nevertheless the high level of trapped porosity within the resulting α grains can only be removed by sintering at temperatures comparable to those used for sintering conventional α alumina powders.

6. Appendix

Fig. 8 shows a cross-section of the toroidal pore, and the area A of the advancing spherical cap of height l is given by:

$$A = 2\pi L_c l \tag{A1}$$

where L_c is a constant (see text) given by Equation 4.

The volume V of the spherical cap is:

$$V = \tfrac{1}{3}\pi l^2 (3L_c - l).$$

When the spherical cap advances a distance dy, the increase in area A is from Equation A1:

$$\mathrm{d}A = 2\pi L_c \mathrm{d}l, \tag{A2}$$

and the volume dV swept through is

$$\mathrm{d}V = \pi l(2L_c - l)\,\mathrm{d}l + \pi r^2\,\mathrm{d}y \tag{A3}$$

where the parameters r and y are depicted in Fig. 8.

Now $r^2 = l(2L_c - l)$ and substituting for r in Equation A3 gives

$$\mathrm{d}V = \pi r^2(\mathrm{d}l + \mathrm{d}y). \tag{A4}$$

Using Equations A2 and A4, condition 5 in the paper can be written

$$(\Delta G_v + \bar{\epsilon}_\theta)\pi r^2(\mathrm{d}l + \mathrm{d}y) - \gamma_{\alpha\theta} 2\pi L_c \mathrm{d}l \geqslant 0. \tag{A5}$$

Since d$l = \tan\phi$ dr, d$y = \cot\psi$ dr and $r = L_c \sin\phi$ and using Equation 4 this condition becomes

$$\frac{4\pi\gamma_{\alpha\theta}{}^2}{(\Delta G_v + \bar{\epsilon}_\theta)}\{\cos^2\phi \tan\phi - \sin^2\phi \cot\psi\} \leqslant 0. \tag{A6}$$

References

1. B. C. LIPPENS and J. H. DEBOER, *Acta. Cryst.* **17** (1964) 1312.
2. R. K. ILER, *J. Amer. Ceram. Soc.* **44** (1961) 618.
3. D. J. STIRLAND, A. G. THOMAS and N. C. MOORE, *Trans. Brit. Ceramic Soc.* **57** (1958) 69.
4. D. I. MATKIN, W. MUNRO and T. M. VALENTINE, *J. Mater. Sci.* **6** (1971) 974.
5. P. A. BADKAR, J. E. BAILEY and H. A. BARKER, *Trans. Brit. Ceramic Soc.* **71** (1972) 193.
6. P. A. BADKAR, J. E. BAILEY and H. A. BARKER, "Materials Science Research", Vol. 6 edited by G. C. Kuczynski (Plenum Press, New York, 1973) p. 311.
7. J. BUGOSH, J., R. L. BROWN, J. R. MCWHORTER, G. W. SEARS and R. J. SIPPEL, "Ultrafine Particles", edited by W. E. Kuhn (Wiley, New York, 1963) p. 206.

8. D. R. ASHWORTH, *J. Brit. Ceram. Soc.* 6 (1969) 70.
9. A. D. CUNNINGHAM and F. W. WILBURN, "Differential Thermal Analysis" Vol. 1, edited by R. C. Mackenzie (Academic Press, London, 1970) p. 49.
10. D. J. BARBER, *J. Mater. Sci.* **5** (1970) 1.
11. B. C. LIPPENS, Thesis Delft Uitgevij Waltman, Delft (1961).
12. R. C. MACKENZIE and G. BÉRGGREN, "Differential Thermal Analysis", Vol. 1, edited by R. C. Mackenzie (Academic Press, London 1970) p. 279.
13. J. YAKOKAWA and O. J. KLEPPA, *J. Phys. Chem.* **68** (1964) 3246.
14. JANAF "Thermochemical Tables", edited by D. R. Stull and H. Prophet (Nat. Bur. Stand., 1971) NSRDS - NBS 37.
15. P. A. BADKAR, Ph. D. Thesis, University of Surrey (1974).
16. M. PLUMMER, *J. Appl. Chem. (London)* 8 (1958) 35.
17. C. S. SMITH *Trans. Met. Soc.* **AIME** 175 (1948) 15.
18. L. H. VAN VLACK, *Trans. Met. Soc. AIME* **191** (1951) 251.
19. D. MCLEAN, "Grain Boundaries in Metals" (Clarendon Press, Oxford, 1957).
20. D. T. LIVEY and P. MURRAY, *J. Amer. Ceram. Soc.* 39 (1956) 363.
21. P. G. SHEWMON, *Trans. Met. Soc. AIME* **233** (1965) 736.
22. G. C. KUCZYNSKI, *Acta. Met.* 4 (1956) 58.
23. D. TURNBULL, *Trans. Met. Soc. AIME* **191** (1951) 661.
24. P. A. BECK, P. R. SPERRY and H. HU, *J. Appl. Phys.* **21** (1950) 420.
25. J. E. BURKE, *J. Amer. Ceram. Soc.* **40** (1957) 80.
26. R. L. COBLE and J. E. BURKE, "Progress in Ceramic Science" Vol. 3, edited by J. E. Burke (Pergamon Press, Oxford, 1963) p. 197.

Received 15 March and accepted 22 March 1976.